

How individual vs shared coordination governs the degree of correlation in rotational vs residence times in a high-viscosity lithium electrolyte

Vinay Thakur,[†] Prabhat Prakash,^{*,†,‡} and Raghavan Ranganathan^{*,†}

[†]*Department of Materials Engineering, Indian Institute of Technology Gandhinagar,
Gujarat, 382355, India*

[‡]*Chemistry and Chemical Engineering, California Institute of Technology, Pasadena,
California, 91125 United States*

E-mail: pprakash@caltech.edu; rraghav@iitgn.ac.in

Abstract

Commercially used carbonate-based electrolytes in lithium-ion batteries are susceptible to many challenges, including flammability, volatility, and lower thermal stability compared to LiTFSI-glyme based electrolytes. Mixtures of LiTFSI salt (lithium bis(trifluoromethylsulfonyl)-amide) and glyme-based solvents are potential alternative candidates for commonly used electrolytes. We perform classical molecular dynamics (MD) simulations to study the effect of concentration and temperature on the translational and rotational dynamics. The radial distribution function shows stronger coordination of Li^+ ions with tetraglyme(G4), as shown in earlier studies, and forms a stable $[\text{Li}(\text{G4})]^+$ cation complex. The self-diffusion coefficients are lower than the values experimentally observed but show improvement over other classical force fields,

without charge scaling. An increase in the salt concentrations leads to a higher viscosity of the system and reduces the overall ionic mobility of Li^+ ions. Diluting the system with a larger number of G4 molecules leads to shorter rotational relaxation times for both TFSI and G4. Ion-residence times show that Li^+ ions form stable and long-lasting complexes with G4 molecules than TFSI anions. The residence time of $[\text{Li}(\text{G4})]^+$ complex increases in highly concentrated system due to the availability of fewer G4 molecules to coordinate with a Li^+ ion. G4 is also seen to form polydentate complexes with Li^+ ions without a shared coordination, allowing rotation without breaking coordination, unlike TFSI, which requires coordination disruption for rotation. This distinction explains the poor correlation between rotation and residence time for G4 and the strong correlation for TFSI.

Introduction

The growing demand for clean energy across the world requires efficient energy storage devices. Batteries and supercapacitors are among the widely used electrochemical devices for energy storage. Lithium-ion batteries (LIBs) have made significant progress in the past three decades in reducing their overall cost with an increase in energy density. The cost has decreased from \$1,000 per kWh in 2009 to \$180 per kWh in 2020, while the energy density has increased from 125 Wh/kg to 250 Wh/kg. The LIB market was \$36.7 billion in 2019 and is expected to reach \$128.3 billion by 2027, with an estimated compound annual growth rate of 18% from 2020 to 2027.^{1,2} The electrolyte is an important component of batteries that determines the cyclic efficiency and the charge-discharge rate of a battery. Generally, ideal electrolytes should possess high ionic conductivity and good electrochemical and thermal stability. Commercialized LIBs use electrolytes of fluoride salts and organic solvents, which provide high ionic conductivity but are susceptible to leakages and flammability and are responsible for most fire accidents in electric vehicles. Various alternative electrolyte systems, such as ionic liquids (ILs),³ solvate ionic liquids (SILs),⁴ polymer electrolytes,⁵ localized

highly concentrated electrolytes,⁶ inorganic solid electrolytes,⁷ soft-solid electrolytes,⁸ and composite electrolytes,⁹ have been proposed to increase the safety aspects and energy density of the batteries. SILs are considered an alternative to conventional organic electrolytes owing to their unique structural characteristics and higher ionic conductivity. SILs generally formed in equimolar mixtures when a cation (e.g., Li^+ here) forms a coordinated complex ($[\text{Li}(\text{G4})]^+$) with the donor sites of the solvent molecule, with anions being solvent-separated and occupying the interstitial volume. SILs have higher viscosity compared to organic electrolytes, still they possess higher ionic conductivity which is attributed to the higher concentration of $\text{Li}(\text{G4})[\text{TFSI}]$.^{10,11} The glyme family of solvents, specifically those with higher chain lengths, are a better alternative to organic solvents in ILs due to their lower flammability, less toxicity, and higher thermal stability. In ILs, the currently used higher chain length solvents are triglyme (G3), tetraglyme (G4), and pentaglyme (G5) with LiTFSI and LiPF_6 salts. LiTFSI salt shows excellent thermal and chemical stability up to 360 °C and dissociates easily in various types of solvents.^{12–16}

Higher chain-length glyme molecules have better physiochemical properties compared to shorter chain-length glyme molecules. Equimolar concentrations of triglyme (G3) and tetraglyme (G4) have been investigated with lithium salts using various experimental (Raman spectroscopy, Small angle X-Ray Scattering, Diffusion nuclear magnetic resonance) and computational techniques.^{10,17,18} Structural properties like radial distribution function (RDF) and radius of gyration (R_g) are useful in predicting the local solvation shell and compactness of atoms or molecules, respectively. The local structure of Li^+ ions prefers to remain in a five-fold (or four-fold) coordination with oxygen of G4 and TFSI combined, where the major contribution comes from G4.^{19–21} Based on G4 or TFSI coordination, the $\text{LiTFSI}/\text{G4}$ complexes are classified as contact ion pairs (CIP) and solvent-separated ion pairs (SSIP). In CIP, oxygen atoms on TFSI directly coordinate with solvated Li^+ ions, whereas in SSIP, TFSI anions interact with the $[\text{Li}(\text{G4})]^+$ complex. The SSIP configurations were found to be energetically more favorable compared to CIP, stating that Li^+ ions prefer to remain as a

$[\text{Li}(\text{G4})]^+$ complex in the system, also supported by the diffusivity ratio ($D_{\text{Li}^+}/D_{\text{G4}}$), which is equal to one for equimolar systems.^{17,22,23}

Experimental techniques like 2D IR spectroscopy, along with molecular mechanics-based non-reactive classical molecular dynamics (MD) simulations and first principle calculations, have been used to assess and characterize the distribution of these various structural complexes.^{20,24–28} However, the challenge with classical MD is that it does not capture the structural changes in solvated structures during the dynamics very well compared to Ab initio (AIMD) simulations. Still, inaccessibility to longer timescales in AIMD simulations forces the use of classical models, especially for longer time-correlated properties like translational and rotational diffusion. Recently, machine learning interatomic potentials (MLIPs) have emerged as an efficient alternative to both classical and ab initio molecular dynamics for liquid electrolytes simulations in batteries. These models can achieve near-first-principles accuracy while dealing with large system sizes and longer timescales accessible to classical MD.^{29–32}

Experimentally, the diffusion coefficients for Li^+ , TFSI, and G4 are calculated at 30 °C and 80 °C (discussed later in the subsection *Translational dynamics*).^{10,18,22,33} Using MD simulations with a polarizable force field, Dong et al.¹⁶ found that the diffusion coefficients of species at 30 °C and 80 °C are one or two order of magnitude less than the experimental diffusion coefficients. Other research groups also used non-polarizable OPLS-force fields with scaled charges (to include polarization effects) and found similar diffusion coefficients at 227 °C.³⁴ No experimental study has been done so far that highlights the system dynamics at such elevated temperatures.³³ The use of scaled charges can model the structure right by over-simplification of the many-body interactions. Thus, the use of more robust methods to compute the partial charge of molecules is required. Dong's group also calculated the lifetime of the Li^+ ions with TFSI and G4 at 373 K, which depends upon the salt concentration. A smaller concentration of salt leads to a greater number of free glyme molecules in the system, which goes through a faster exchange event with glyme molecules binding with

Li^+ ions, thus reducing the lifetime of the $\text{Li-O}_{\text{G}4}$.¹⁶ The translation diffusion, exchange events, and residence times also dictate the coiling and bending of geometries of G4 and TFSI, respectively. However, no modeling of rotational dynamics has been conducted yet that shows the effect of the coiling/bending of one molecule on another or on the rotational lifetime of molecules. The rotational contribution is an important factor in deciding the lifetime of big continuous clusters of Li^+ ions with TFSI and G4. Moreover, the effect of correlated motions on the ionic mobility is not very well understood even in some of the recent studies,^{35–37} which motivates us to investigate if there is an interplay between residence and rotational lifetimes in such high-viscosity lithium electrolytes. Although, the absolute timescales might be overestimated due to simulation limitations, the observed relative trends and the correlation between residence and rotational times are expected to be reliable and physically meaningful.

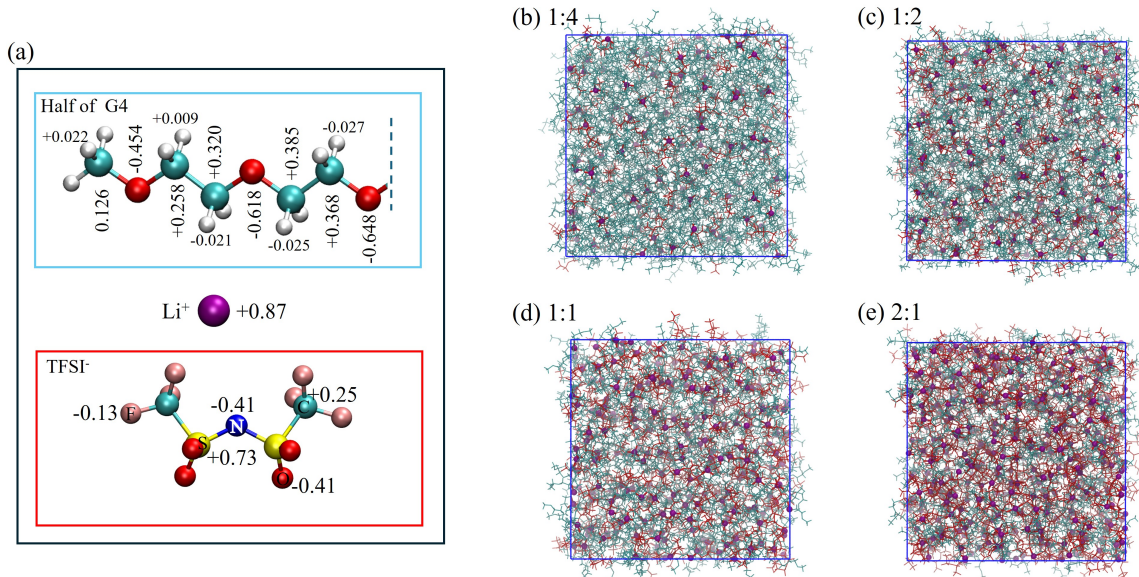


Figure 1: (a) Schematic representation of LiTFSI and G4 with partial atomic charges, (b) 1:4, (c) 1:2, (d) 1:1 and (e) 2:1 ratio mixtures of LiTFSI/G4 at 300 K after an equilibration of 10 ns.

This study investigates the extreme range of LiTFSI and G4 mixture compositions (from 1:4 to 2:1) at various temperatures with classical MD simulations using a modified OPLS

force-field.³⁸ The partial charges for atoms of LiTFSI and G4 are reparametrized here (Fig. 1). A correct structure prediction and long timescale simulations performed in the present work provide a reliable set of results for diffusion coefficients, residence times, rotational relaxation times, and cluster sizes and theorize a not-yet-explored interplay of these.

Computational Details

Four mixtures with different LiTFSI/G4 ratios (1:4, 1:2, 1:1, and 2:1) were studied, as shown in Table S1 of supplementary information. These mixtures were modeled using a charge-reparameterized OPLS force field. Partial atomic charges for the LiTFSI and G4 molecules were calculated (Fig. 1a) using a range-separated hybrid functional wB97x-D4 functional^{39,40} with a sufficiently large basis set def2-tzvpp, utilizing the ORCA 5.0.1 package.⁴¹ Partial atomic charges were derived for all atoms of TFSI and G4 from their geometries in Li-bonded states using CHELPG method.⁴² A fixed charge of +0.87 was assigned to Li⁺ ions based on the bonded state of the cation and free cation. The PME⁴³ algorithm was used to compute the long-range electrostatic interactions. The cut-off for Lennard-Jones and electrostatic interactions is set to 10 Å. A time-step of 1 femtosecond is used throughout the simulations. All simulations were conducted using the Gromacs 2021⁴⁴ software package. For post-processing and analysis, VMD 1.9.3,⁴⁵ Travis,⁴⁶ and in-house scripts developed in python were used.

The different ratio mixtures were initially minimized using the conjugate-gradient algorithm. Each system was heated from 300 K to 600 K in the NPT ensemble with a heating rate of 50 K per 5 ns to mix it well, followed by an equilibration run in the NVT ensemble for 10 ns at each particular temperature. Fig. 1(b-e) shows post-equilibrated mixtures at 300 K. Velocity rescaling method⁴⁷ and Berendsen barostat⁴⁸ were used to manage fluctuations in temperature and pressure, respectively. Following this, the systems were cooled again from 600 K to 300 K in the NPT ensemble at the interval of 50 K per 5 ns with 10 ns of NVT

equilibration at each particular temperature. Final production runs were performed at 300 K and 500 K in NVT ensemble conditions for 100 ns to obtain sufficiently long trajectories for analysis.

Results and discussion

Solvation structure

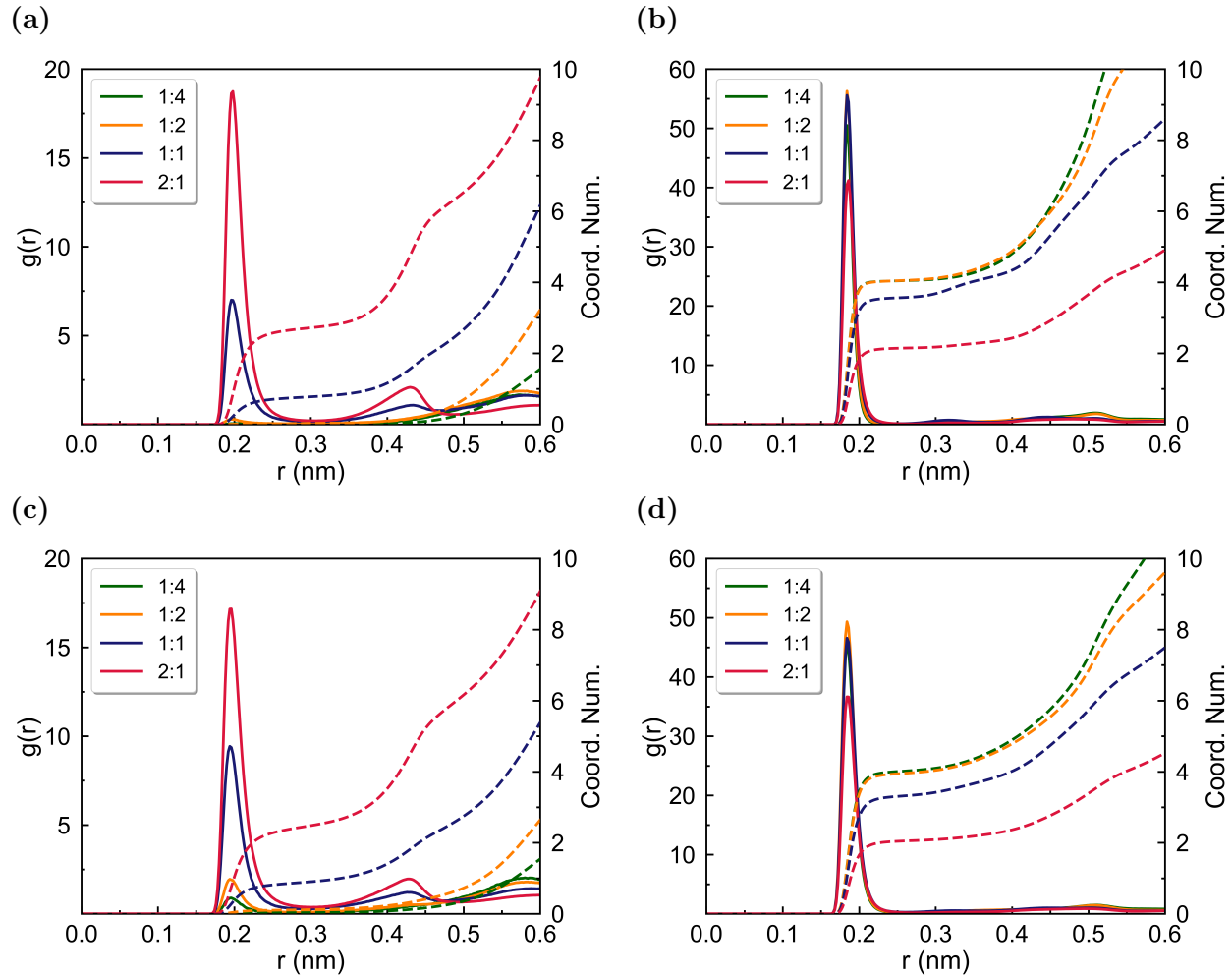


Figure 2: Radial distribution function for (a) Li...O(TFSI), (b) Li...O(G4) at 300 K, and (c) Li...O(TFSI), (d) Li...O(G4) at 500 K for different compositions.

The interatomic interactions of TFSI and G4 around Li^+ ions are calculated as radial distribution functions (RDF):

$$g(r) = \frac{n(r)}{\rho 4\pi r^2 \Delta r} \quad (1)$$

$$n(r') = 4\pi\rho \int_0^{r'} g(r)r^2 dr \quad (2)$$

where $g(r)$ is RDF, $n(r)$ is the number of particles located at the distance between r and $r + \Delta r$ from the reference particle, ρ is the bulk number density, and r' is the distance of the first minima of $g(r)$ from each atom. The coordination number $n(r')$ is calculated by integrating the RDF over the chosen spherical shell around the central atom. The neutron scattering confirms that in an equimolar mixture of LiTFSI and G4, 95 % G4 molecules are coordinated by Li^+ ions and the remaining 5 % have an incomplete $\text{Li} \dots \text{O}(\text{G4})$ coordination.⁴⁹ The experimental $g(r)$ peaks are observed at 1.9 Å for $\text{Li} \dots \text{O}(\text{G4})$, and 2.0 Å for $\text{Li} \dots \text{O}(\text{TFSI})$ in an equimolar (1:1) mixture.⁴⁹ Our simulations are in a good agreement with these observations as the first solvation shell of a Li^+ ion is seen to form at 1.9 Å with O atoms of G4 and at 2.0 Å with O atoms of TFSI (Fig. 2). From the integration of these RDFs (within a cut-off radius of 2.3 Å), the coordination number in the equimolar ratio at 300 K is 3.6 for $\text{Li} \dots \text{O}(\text{G4})$ and $\simeq 0.7$ for $\text{Li} \dots \text{O}(\text{TFSI})$. The variation in the coordination number of Li^+ ions is observed at different salt concentrations. With the increase in the concentration of glyme molecules, the coordination number of $\text{Li} \dots \text{O}(\text{G4})$ increases nearly to 4 at 1:2 and 1:4 ratios. Also, the increase in the concentration of solvent leads to an increase in the intensity of RDF of the $\text{Li} \dots \text{O}(\text{G4})$, whereas the intensity of RDF of $\text{Li} \dots \text{O}(\text{TFSI})$ decreases as more number of Li^+ ions find free G4 and get attached to them. Changing the concentration of salt and solvent does not affect the radius of the first coordination shell around lithium.

The coordination number of $\text{Li} \dots \text{O}(\text{G4})$ in equimolar ratio decreased to 3.3 (500 K) from 3.6 (300 K). This could happen due to the accelerated dynamics, which leads to a faster exchange between G4 molecules at higher temperatures within the solvation shell of lithium.

This also leads to a decrease in the lifetime of Li...O(G4) complex which is confirmed through ion-pair/ion-solvent existence autocorrelation function (discussed *vide infra* in subsection *Ion-residence times*). Also, the intensity of RDF peaks showed a small decrease at 500 K for both Li...O(TFSI) and Li...O(G4) when compared to RDF at 300 K.

Radius of gyration

Since both the TFSI anion and G4 are long molecular structures, their coiling leads to a significant variation in the radii of gyration (R_g). The R_g of these species is an important factor that is sensitive to the temperature and concentration of electrolyte mixture. We used MD trajectories to calculate R_g for TFSI anions and G4 molecules for each ratio and at 300 K and 500 K (Fig. S2 and S3 in supplementary information). As shown in Table 1, the R_g of TFSI and G4 in the most diluted system (1:4) at 300 K is, 0.256 nm and 0.381 nm, respectively. At a higher concentration, 2:1, the R_g for both TFSI and G4 decreases to 0.254 nm and 0.363 nm, suggesting a more coiled configuration, particularly for G4, which shrinks by 5 %. The R_g for both TFSI and G4 decrease in highly concentrated system. This indicates that at higher salt concentrations, most G4 molecules coordinate individually with the Li^+ ions, thus increasing their overall compactness. In diluted system, there are more free G4 molecules available to share the coordination leading to higher R_g . As expected at higher temperature, R_g for TFSI and G4 increase from 0.256 nm to 0.257 nm and from 0.381 nm to 0.387 nm respectively, when increasing the temperature from 300 K to 500 K. Even these slight changes in R_g is an important factor which can lead to an interplay in translational and rotational dynamics and ion-residence times in these mixtures (discussed *vide infra*).

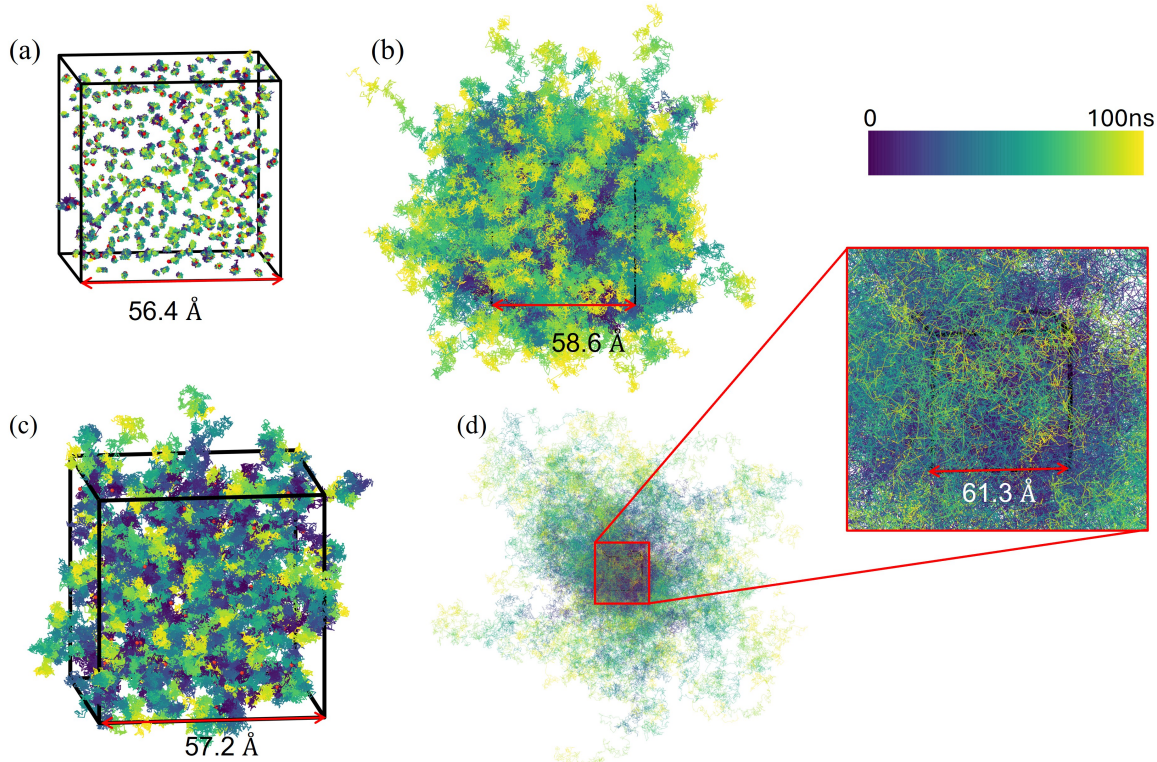


Figure 3: Trajectory of Li^+ ions over a time of 100 ns for different LiTFSI/G4 ratios (a) 2:1 at 300 K, (b) 2:1 at 500 K, (c) 1:4 at 300 K, (d) 1:4 at 500 K.

Table 1: Average and standard deviation of radius of gyration, $R_g(\text{nm})$, for 1:4 and 2:1 system

	Species	Temp (300 K)		Temp (500 K)	
		Average	Std. dev.	Average	Std. dev.
1:4	TFSI	0.256	0.0006	0.257	0.0006
	G4	0.381	0.0016	0.389	0.0018
2:1	TFSI	0.254	0.0002	0.255	0.0003
	G4	0.363	0.0007	0.367	0.0034

Translational dynamics

The translational diffusion of ions and G4 is ascertained with the calculation of mean square displacement (MSD) for all trajectories. Since Li^+ ions are strongly coordinated with O atoms of TFSI and G4, at high-concentration (e.g., 2:1) and low-temperature (e.g. 300 K), their movement (Li^+ ions) is heavily vibrational in their coordination ‘cage’. The trajectory

Table 2: Comparison of self-diffusion coefficients, D (in 10^{-7} cm 2 /s), for equimolar (1:1) LiTFSI/G4 electrolyte reported in various experimental and MD simulations works

Temp (K)	D_{Li^+}	D_{TFSI^-}	D_{G4}
^a <i>Experiments - Tamura et al.</i> ¹⁰			
303	1.26	1.22	1.26
^a <i>Experiments - Yoshida et al.</i> ⁵⁰			
303	1.31	1.22	1.29
^a <i>Experiments - Zhang et al.</i> ²²			
303	1.26	1.22	1.26
^a <i>Experiments - Harte et al.</i> ³³			
303	1.01	1.04	0.87
353	27.90	7.08	6.33
^b <i>MD Simulations - Dong et al.</i> ¹⁶			
303	0.41	0.40	0.41
^c <i>MD Simulations - Tsuzuki et al.</i> ¹⁹			
403	0.78	0.73	0.78
^c <i>MD Simulations - Shinoda et al.</i> ⁵¹			
503	4.5	5.7	4.6
^d <i>MD Simulations - Thum et al.</i> ³⁴			
500	53	59	54
^e <i>MD Simulations - Harte et al.</i> ³³			
500	52.02(± 1.06)	56.63(± 3.23)	53.10(± 1.46)
700	96.16(± 16.02)	113.12(± 6.56)	96.69(± 10.69)
^f <i>MD Simulations - This work</i>			
300	0.02(± 0.01)	0.04	0.03(± 0.01)
500	12.43(± 0.27)	23.7(± 2.51)	12.38(± 0.02)

^aPFG-NMR

^bMD simulation, polarizable APPLE&P force field

^cMD simulation, OPLS-AA and CL&P force field, no charge scaling

^dMD simulation, OPLS-AA and CL&P force field, with scaled charges

^eMD simulation, OPLS-AA force field, with scaled charges

^fMD simulation, OPLS-AA force field, no charge scaling

lines for 2:1 and 1:4 compositions (Fig. 3) at 300 K and 500 K show that for 2:1 at 300 K (Fig. 3a), all Li^+ ions move in the coordination cage with a vibrational motion of 0.1 - 0.3 Å of amplitude between two frames separated over 5 ps time-interval. These cage-vibrations are also observed in other inorganic and soft-solid electrolytes^{8,52}. The self-diffusion coefficients (D) are obtained from the diffusive regime of MSD vs time plots (refer to Fig. S4 and S5 in supplementary information), utilizing the Einstein relationship as:

$$D = \frac{1}{2d\Delta t} \frac{1}{N} \sum_{i=1}^N \langle (|r_i(t + \Delta t) - r_i(t)|^2) \rangle \quad (3)$$

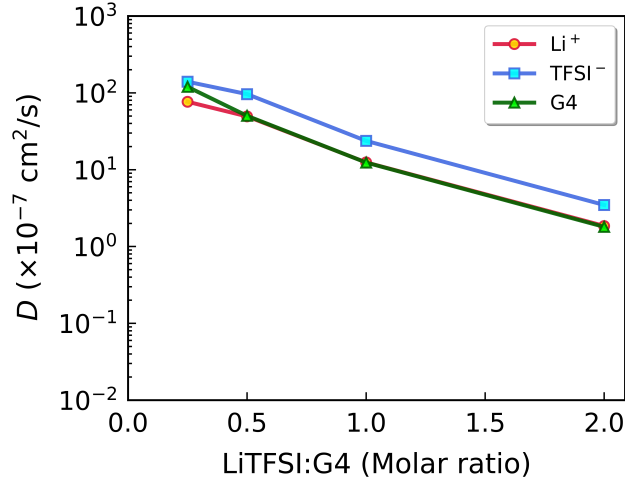


Figure 4: Self-diffusion coefficients of Li^+ , TFSI^- , and G4 for different LiTFSI/G4 ratios at 500 K

Here, $r_i(t)$ is the position of i th atom at time t , Δt is the lag time, d is the dimensionality of the system, N is the number of particles, and $\langle (|r_i(t + \Delta t) - r_i(t)|^2) \rangle$ is the mean square displacement average over multiple times origin. The calculated values of self-diffusion coefficients at 300 K and 500 K are reported in Table S2 of the supplementary information, and are provided in Fig. 4 (at 500 K). Experimentally, the self-diffusion coefficient of Li^+ ions (D_{Li^+}) is measured using both impedance spectroscopy and pulsed-field gradient NMR (Table 2).^{18,22,33} In simulations, classical MD with scaled charges (a brute-force way to obtain the appropriate local interactions and diffusion) predicts self-diffusion coefficients better

than the other non-scaled charge-based works.^{33,34} Here, the diffusion coefficients of G4 are similar to those of Li^+ ions for a 1:1 system, showing the formation of stable $[\text{Li}(\text{G4})]^+$ complexes. This suggests that lithium primarily diffuse in "vehicular-type" mechanism, in the form of $[\text{Li}(\text{G4})]^+$ complex.^{22,23} With more G4 molecules available in the mixture, D_{Li^+} , D_{TFSI^-} and D_{G_4} increase due to faster exchanges between G4 molecules inside Li^+ ion solvation shell. We also calculated $\text{Li} \dots \text{Li}$ radial distribution functions, RDFs, (Fig. S1 in supplementary information) which show that the most probable distance between two Li^+ ions is 4-6 Å, similar to what is observed in highly concentrated solid electrolytes.^{8,53} This includes the possibility of hopping between transient coordination sites along with vehicular motion, leading to sluggish diffusion of Li^+ ions. Also, increasing the concentration of LiTFSI leads to an increase in the pairing probability of $[\text{Li}(\text{G4})]^+$ and TFSI anions, causing sluggish diffusion of both ions.²¹ The calculated transference numbers for Li^+ are close to 0.34 (Table S3), considering no anion-blocking, thus are closer to PFG-NMR value (~ 0.5) while significantly overestimated compared to potentiostatic polarization estimates (0.02 - 0.03).^{54,55}

Rotational dynamics

The rotational autocorrelation function (RACF) is employed to analyze the orientational dynamics of TFSI and G4. In the case of TFSI anion, a specific atom triplet is selected, comprising S-N-S atoms. A vector is defined by taking the cross-product of the two vectors connecting the S-N and N-S atoms. Similarly, for the G4 molecule, the atom triplet consists of C-O-C atoms, where O is the central oxygen atom of the chain. The RACF for the vector is written as

$$C(t) = \langle (u(0) \cdot u(t)) \rangle \quad (4)$$

where $u(0)$ and $u(t)$ are the vectors chosen for molecules at time $t = 0$ and $t = t$.

Fig. S6 in supplementary information shows that for the system with the highest concentration of G4 molecules (1:4), RACF for both TFSI and G4 decays slower with increasing salt concentration. In dilute mixtures, larger number of free G4 molecules in the system are partially/not coordinated with Li^+ ions, resulting in fewer obstructions in their rotational dynamics. Also, viscosity in LiTFSI-based electrolytes rises with increasing LiTFSI concentration but decreases significantly with the temperature rise, with reports indicating a reduction of up to 83 % in few cases and more than that, over a 50 K temprature rise.^{56,57} With increasing salt concentration, the rotational decay becomes much slower, due to the higher viscosity of the system and increase in the shared coordination of TFSI and G4 with Li^+ ions. Also, G4 molecules rotate more slowly than TFSI anions, primarily due to a bigger radius of gyration and also due to their higher coordination with Li^+ ions.

The rotational relaxation time τ_{rot} (Table 3) is calculated as

$$\tau_{rot} = \int_0^\infty C(t) dt \quad (5)$$

At 300 K, the $C(t)$ for some compositions did not decay sufficiently during the simulation time; hence τ_{rot} for those is calculated analytically here by fitting $C(t)$ with two exponential functions, with the fitting coefficients shown in Table S4 and S5 in supplementary information. At 300 K, τ_{rot} is 295 ns for TFSI and 893 ns for G4 for 2:1 mixture. As the amount of G4 increases, τ_{rot} decreases sharply for both TFSI and G4. τ_{rot} at 300 K is in the order of ns which decreases to ps as the temperature is raised to 500 K. The local structure and the nature of coordination of Li^+ ions alters τ_{rot} for a couple of orders across these concentrations. An analysis on the correlation of τ_{rot} with the residence time of G4...Li and TFSI...Li and formation of interatomic networks (clusters) is discussed further to understand this complexity.

Table 3: Rotational relaxation time, τ_{rot} (ns), for TFSI and G4 for different concentrations at 300 K and 500 K

	Temp (300 K)		Temp (500 K)	
	$\tau_{\text{rot,TFSI}}$	$\tau_{\text{rot,G4}}$	$\tau_{\text{rot,TFSI}}$	$\tau_{\text{rot,G4}}$
1:4	0.2	6.02	0.005	0.03
1:2	0.59	22.59	0.005	0.06
1:1	15.7	189.15	0.020	0.16
2:1	295.22	893.31	0.260	0.59

Ion-residence times

The ion-residence times are calculated for Li^+ ions with TFSI and G4 as the duration which a Li^+ ion would spend with a TFSI anion or a G4 molecule before completely breaking away from the interaction. The residence time of Li^+ aggregates formed with TFSI and G4 is computed as an ion-pair (or ion-solvent) existence autocorrelation function (IEAF), which can be written as an auxiliary function

$$\beta_{ij}(t) = \begin{cases} 1, & \text{TFSI and G4 inside Li}^+ \text{ solvation shell} \\ 0, & \text{otherwise} \end{cases} \quad (6)$$

and the IEAF for β_{ij} is

$$C(t) = \frac{1}{N^2} \sum_{i=1}^N \sum_{j=1}^N \int_0^\infty \beta_{ij}(t) \cdot \beta_{ij}(t + \tau) dt \quad (7)$$

The residence time τ_{res} of the aggregates formed can be computed by twice the integral of IEAF

$$\tau_{\text{res}} = 2 \int_0^\infty C(t) dt \quad (8)$$

τ_{res} for $\text{Li} \dots \text{O}(\text{G4})$ and $\text{Li} \dots \text{O}(\text{TFSI})$ interactions is calculated within the first solvation shell of lithium. The radius of the solvation shell is taken from the first minima of the corresponding RDFs. Fig. S7 in supplementary information shows the decay of IEAF for

Li-O, for both TFSI and G4 at 300 K and 500 K. The decay is too sluggish for Li...O(TFSI) and Li...O(G4) in highly concentrated system. For all these systems τ_{res} is calculated numerically (for well-decayed) and analytically (for sluggish-decayed) tabulated in Table S6 on the supplementary information. The value of τ_{res} is $\sim 6 \mu\text{s}$ for Li...TFSI and $\sim 30 \mu\text{s}$ for Li...G4 for 2:1 mixture at 300 K, which decreases to $\sim 1 \text{ ns}$ and $\sim 882 \text{ ns}$, respectively, as the system is diluted with more G4 (1:4). Dong et al.¹⁶ calculated the residence time of Li...O(TFSI) at various temperatures and showed that, for the 1:1 system, the residence time for Li...O(TFSI) is $\sim 7 \text{ ns}$ at 303 K and decreases with increasing the concentration of free G4 molecules and at higher temperatures. In our study, for equimolar system, the residence time of Li...O(TFSI) is 445 ns at 300 K and decreased to 1 ns at 500 K, as shown in Table S6 in the supplementary information. Similarly, the residence time of Li...O(G4) is $\sim 34 \mu\text{s}$ at 300 K and decreases by three orders to $\sim 46 \text{ ns}$ at 500 K. The discrepancy in the residence time between our study and Dong's group could be due to the differences in force fields and the treatment of partial charges. They used polarizable force field that capture the dynamic molecular charge redistribution in response to the changing environment, which in turn weakens the coordination, facilitates exchange, and consequently reduces the residence time. In a similar study for an equimolar LiTFSI/G4, Shinoda et al.⁵¹ reported that the residence time of Li...TFSI and Li...G4 at 503 K was 2.5 ns and 87 ns, respectively, which is closure to the values we observed. The slight differences may be due to differences in how partial charges were assigned. More dilution leads to an increase in the number of free G4 molecules in the system, enabling their rapid exchange with the Li⁺ ion coordination shell, subsequently decreasing the residence time.

We propose that such long-residence times, particularly at high concentration and low temperature, could affect the rotational motion of these entities with a significantly large R_g . If an ion-solvent or ion-pair network has a long lifetime (τ_{res}), then their τ_{rot} would also be proportionately longer. To probe this, we computed the correlation of τ_{res} and τ_{rot} for each G4 and TFSI, at 300 K and 500 K. Here each dataset has four pairs of values for

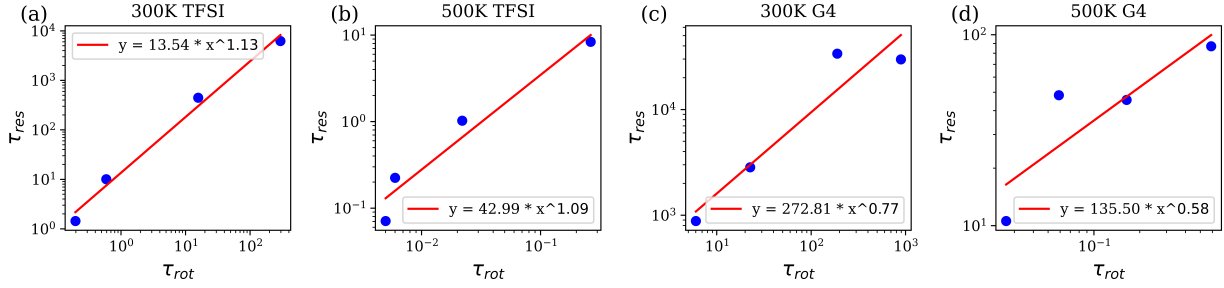


Figure 5: Correlation plots for τ_{res} vs. τ_{rot} of (a) TFSI at 300 K, (b) TFSI at 500 K, (c) G4 at 300 K, (d) G4 at 500 K.

the different concentrations of G4 and TFSI. Plotted on a log-log scale (Fig. 5), lifetimes (rotational-individual and residence with Li) of TFSI anion are fitted as $x^{1.13}$ and $x^{1.09}$ at 300 K and 500 K, respectively - exhibiting a greater than 99% correlation in both cases of temperature. However, for G4, there is surprisingly low-correlation of 66% (at 300 K) and 89% (at 500 K) between the lifetimes. It can be understood that an increase from 300 K to 500 K in temperature simply aligns the rotational motion with the residence time better, but there is a stark contrast of this correlation with TFSI. To investigate further, we analyzed ionic aggregates, most-probable clusters and their nature below.

Ionic aggregates and clusters

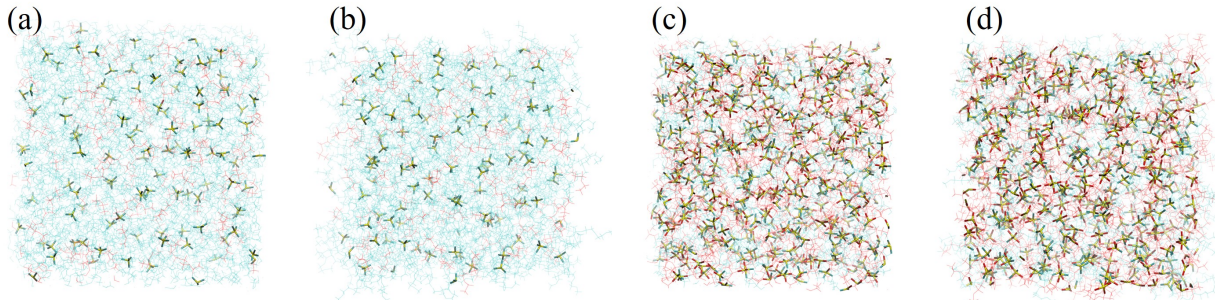


Figure 6: Dynamic bonds $\leq 2.3 \text{ \AA}$ showing Li...O(G4) (yellow-green) and Li...O(TFSI) (yellow-red) clusters in LiTFSI/G4 molar ratios (a) 1:4 at 300 K, (b) 1:4 at 500 K, (c) 2:1 at 300 K, and (d) 2:1 at 500 K. Thick lines, yellow Li, red O(TFSI), green O(G4); Thin lines, red TFSI, green G4.

All the concentrations of LiTFSI/G4 are observed to form long networks where Li, TFSI

Table 4: Number of uncoordinated molecules of TFSI or G4 and the size of the biggest exclusive clusters of Li...TFSI and Li...G4 at 300K and 500K.

		300K				500K	
		Li-TFSI		Li-G4		Li-TFSI	
		Uncoord.	Size of	Uncoord.	Size of	Uncoord.	Size of
		Max.		Max.		Max.	
1:4	5.7	187.3	0.1	539.9	5.3	172.5	0.4
1:2	7.6	415.1	1.7	645.6	8.4	412.2	2.3
1:1	3	397	0.4	455.5	2.8	436	0.9
2:1	11.5	852.5	4	631.1	8.6	845.2	3

Table 5: Number of uncoordinated molecules (TFSI and/or G4) and size of the biggest shared cluster involving Li..G4, Li...TFSI or G4...Li...TFSI.

	Temp (300 K)		Temp (500 K)	
	Single	Maximum	Single	Maximum
1:4	77.6	569	77.8	553
1:2	147.8	712	122.9	705
1:1	91.5	637	65.2	634
2:1	5.9	1070	9.6	1062

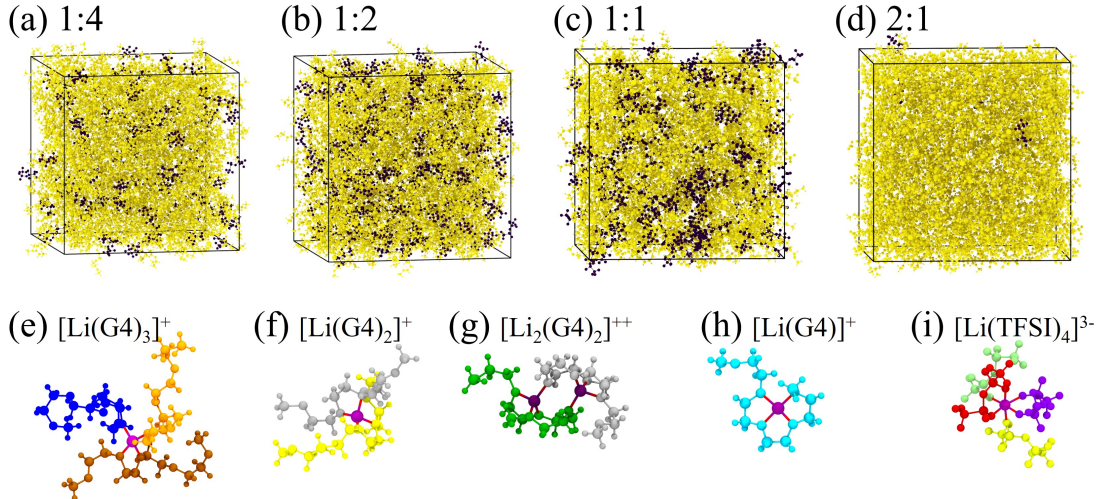


Figure 7: Single largest cluster (in yellow) and all other small clusters (in black) for (a) 1:4, (b) 1:2, (c) 1:1 and (d) 2:1 LITFSI/G4 at 300 K, the snapshots show the uncoordinated molecules (black), in each case, which decrease with concentration; Most probable finite clusters from a trajectory of 90 ns, (e), (f), (g), (h), and (i).

and G4 coordinate in a shared and unshared manner to form various clusters. Fig. 6 shows the dynamic bonds around each Li^+ ion in each case of concentration at 300 K. The snapshots show that for the dilute mixtures (1:4), most of these clusters are individual, and/or unshared (Fig. 6 a, b). For the concentrated mixtures at 2:1 ratio, long-chains, shared coordination lead to the formation of complex aggregates (Fig. 6 c, d). The aggregation of molecules as long vs. short networks is analyzed by calculating the number and size of clusters during the production run for last 90 ns of simulation time. A cut off of 2.3 Å, chosen from RDF, is set as the criteria for cluster formation. We define a cluster when one or more atoms of a G4 or TFSI are within 2.3 Å to a Li^+ ion. We analyzed these networks as two different ways - individual and shared. For individual networks, mutually exclusive $\text{Li} \dots \text{TFSI}$ and $\text{Li} \dots \text{G4}$ clusters are calculated (Table 4). For shared networks, every possible cluster involving Li or G4 or TFSI within 2.3 Å are calculated (Table 5). For these networks, we look at the two extreme conditions : the size of the single largest network and the number of smallest cluster (of size 1, which is essentially an uncoordinated G4 or TFSI). For 1:4 mixture at 300 K, the number of molecules that do not form any cluster is nearly equal to 6 (out of 108) which are mostly TFSI anions. This suggests that in case of excessive solvation with G4, the free uncoordinated molecules are TFSI. For concentrated systems (2:1), ~11 (out of 432) TFSI and 4 (out of 216) G4 molecules are left uncoordinated. The analysis of all (individual+shared) clusters shows that ~14% TFSI or G4 (total 77.6) are uncoordinated and free at 1:4 at 300 K. As the system is more concentrated, this number first increases for 1:2 to 22% and then decreases for more concentrated systems, 18% for 1:1, and less than 1% for 2:1. The largest networks at various concentrations, which involve the majority of TFSI, G4 forming these via a shared coordination with Li^+ ions, are shown in Fig. 7 (a - d).

We obtained some of the prominent finite geometries from these systems (Fig. 7 e - i), which unravel the difference in the degree of correlation in τ_{res} and τ_{rot} of TFSI vs. G4. The key arguments are as follows with the index of subfigures:

(e) For 1:4 system, shared clusters mostly involving multiple G4 around a Li^+ ion are formed;

since only one or rarely two O(G4) coordinate with a Li⁺ ion, the rest O(G4) coordinate with other Li⁺ ions and thus forming a long ... (G4)...Li...(G4)...Li... network, leaving no individual G4 uncoordinated.

(f) For 1:2 system, some G4 bidentate with a Li⁺ ion; the other O(G4) atoms form extended networks similar to 1:4.

(g) For 1:1 system, some Li⁺ ions form close-contact aggregates, which have two Li⁺ ions bidentate by two G4 molecules.

(h) shows single unshared complex of G4 with a Li⁺ ions; such complexes rarely form shared networks, except at high concentrations ($\geq 1:1$), where anions dentate additionally raising the coordination number from 4 to 5 or 6.

(i) shows a Li...TFSI cluster which forms only via shared coordination from multiple TFSI. A single TFSI cannot form a complex like (h) due to rigidity and other geometrical constraints.

It is important to notice here that G4 can form individual unshared complexes with a Li⁺ ion in a polydentate manner, which TFSI cannot. Thus, a rotation of Li...G4 complex can occur without the need of breaking the coordination, while in case of Li...TFSI, break in coordination is essential for any rotation of an individual TFSI. This explains the poor correlation between τ_{rot} and τ_{res} for G4, and highly correlated those for TFSI. A longer residence time only restricts the rotation when there is coordination from multiple similar entities, where the diffusion of Li⁺ ions can have a significant contribution from hopping. A polydentate anion or solvent coordinating in an unshared manner would not affect its rotation with its residence time and thus can live longer while rotating faster. The correlation observed here is potentially an important descriptor, that can be further tested in extending the general theories for concentrated electrolytes^{58,59} to those with long-chain entities.

Conclusion

This work demonstrates the impact of varying salt concentrations and temperature on the structure, dynamics and interplay of residence vs. rotational relaxation times in LiTFSI/G4 mixtures with classical MD simulations. The structural analysis shows that lithium ions preferentially coordinate with glyme molecules, forming $[\text{Li}(\text{G4})]^+$ complexes, complementing the earlier experimental and computational studies. Temperature, in the range of 300 K to 500 K, did not significantly affect the local solvation structure of Li^+ ion, suggesting that the coordination environment remains stable even at higher temperatures. The dynamic properties indicated that the self-diffusion coefficients of Li^+ ions and solvent molecules decreased with increasing salt concentration, resulting in a sluggish movement of ions. This suggests that higher salt concentrations increase the viscosity of the system, thus restricting the overall ionic mobility. In highly concentrated system, a larger network of clusters is formed, which causes sluggish dynamics of the ions and molecules in the system.

The ability of G4 to form individual unshared polydentate complexes with Li^+ allows rotation without breaking coordination, while TFSI must disrupt coordination to rotate. This difference accounts for the varying correlations between rotation and residence time in both cases. A longer residence time restricts rotation only when multiple similar entities coordinate, while a polydentate species with unshared coordination can maintain rapid rotation despite prolonged residence. An experimental examination of this effect could provide valuable insights into the viscosity, ionic conductivity, and thermal stability of LIBs.

Acknowledgement

RR acknowledges funding support from the Department of Science and Technology's National Supercomputing Mission grant DST/NSM/R&D_HPC_Applications/2021/30. The authors acknowledge the Param Shivay (IIT BHU) and Param Ananta (IIT Gandhinagar) supercomputing facilities for the simulations reported in this work.

Supporting Information Available

System size details, additional plots for radii of gyration, lifetimes and mean-squared displacements are provided in the Supporting Information.

References

- (1) Feng, X.; Fang, H.; Wu, N.; Liu, P.; Jena, P.; Nanda, J.; Mitlin, D. Review of modification strategies in emerging inorganic solid-state electrolytes for lithium, sodium, and potassium batteries. *Joule* **2022**, *6*, 543–587.
- (2) Nitta, N.; Wu, F.; Lee, J. T.; Yushin, G. Li-ion battery materials: present and future. *Materials Today* **2015**, *18*, 252–264.
- (3) Rana, S.; Thakur, R. C.; Dosanjh, H. S. Ionic liquids as battery electrolytes for lithium ion batteries: Recent advances and future prospects. *Solid State Ionics* **2023**, *400*, 116340.
- (4) Nachaki, E. O.; Kuroda, D. G. Transitioning from Regular Electrolytes to Solvate Ionic Liquids to High-Concentration Electrolytes: Changes in Transport Properties and Ionic Speciation. *The Journal of Physical Chemistry C* **2024**, *128*, 11522–11533.
- (5) Wu, M.; Han, S.; Liu, S.; Zhao, J.; Xie, W. Fire-safe polymer electrolyte strategies for lithium batteries. *Energy Storage Materials* **2024**, *66*, 103174.
- (6) van Ekeren, W. W.; Albuquerque, M.; Ek, G.; Mogensen, R.; Brant, W. R.; Costa, L. T.; Brandell, D.; Younesi, R. A comparative analysis of the influence of hydrofluoroethers as diluents on solvation structure and electrochemical performance in non-flammable electrolytes. *Journal of Materials Chemistry A* **2023**, *11*, 4111–4125.
- (7) Yu, T.; Liu, Y.; Li, H.; Sun, Y.; Guo, S.; Zhou, H. Ductile Inorganic Solid Electrolytes for All-Solid-State Lithium Batteries. *Chemical Reviews* **2025**, *125*, 3595–3662.

(8) Prakash, P.; Fall, B.; Aguirre, J.; Sonnenberg, L. A.; Chinnam, P. R.; Chereddy, S.; Dikin, D. A.; Venkatnathan, A.; Wunder, S. L.; Zdilla, M. J. A soft co-crystalline solid electrolyte for lithium-ion batteries. *Nature Materials* **2023**, *22*, 627–635.

(9) Zhang, Z.; Wang, X.; Li, X.; Zhao, J.; Liu, G.; Yu, W.; Dong, X.; Wang, J. Review on composite solid electrolytes for solid-state lithium-ion batteries. *Materials Today Sustainability* **2023**, *21*, 100316.

(10) Tamura, T.; Yoshida, K.; Hachida, T.; Tsuchiya, M.; Nakamura, M.; Kazue, Y.; Tachikawa, N.; Dokko, K.; Watanabe, M. Physicochemical properties of glyme-Li salt complexes as a new family of room-temperature ionic liquids. *Chemistry letters* **2010**, *39*, 753–755.

(11) Di Lecce, D.; Marangon, V.; Jung, H.-G.; Tominaga, Y.; Greenbaum, S.; Hassoun, J. Glyme-based electrolytes: suitable solutions for next-generation lithium batteries. *Green Chemistry* **2022**, *24*, 1021–1048.

(12) Wang, Q.; Mao, B.; Stoliarov, S. I.; Sun, J. A review of lithium ion battery failure mechanisms and fire prevention strategies. *Progress in Energy and Combustion Science* **2019**, *73*, 95–131.

(13) Di Lecce, D.; Marangon, V.; Jung, H.-G.; Tominaga, Y.; Greenbaum, S.; Hassoun, J. Glyme-based electrolytes: suitable solutions for next-generation lithium batteries. *Green Chemistry* **2022**, *24*, 1021–1048.

(14) Lingua, G.; Depraetère, G.; Wang, J.; Bara, J. E.; Forsyth, M.; Mecerreyes, D. Solvate Ionic Liquids based on branched glymes enabling high performance lithium metal batteries. *Journal of Power Sources* **2024**, *624*, 235535.

(15) Rajendran, S.; Ganesan, V. S.; Arava, L. M. R. Electrochemical instability of room-temperature ionic liquids with LiTFSI at elevated temperature and its consequences in Li/Li-ion based half-cells and full-cells. *Electrochimica Acta* **2024**, *498*, 144599.

(16) Dong, D.; Bedrov, D. Charge transport in $[\text{Li}(\text{tetraglyme})][\text{bis}(\text{trifluoromethane})\text{sulfonimide}]$ solvate ionic liquids: insight from molecular dynamics simulations. *The Journal of Physical Chemistry B* **2018**, *122*, 9994–10004.

(17) Aguilera, L.; Xiong, S.; Scheers, J.; Matic, A. A structural study of LiTFSI-tetraglyme mixtures: From diluted solutions to solvated ionic liquids. *Journal of Molecular Liquids* **2015**, *210*, 238–242.

(18) Yoshida, K.; Tsuchiya, M.; Tachikawa, N.; Dokko, K.; Watanabe, M. Change from glyme solutions to quasi-ionic liquids for binary mixtures consisting of Lithium Bis(trifluoromethanesulfonyl) amide and Glymes. *The Journal of Physical Chemistry C* **2011**, *115*, 18384–18394.

(19) Tsuzuki, S.; Shinoda, W.; Matsugami, M.; Umebayashi, Y.; Ueno, K.; Mandai, T.; Seki, S.; Dokko, K.; Watanabe, M. Structures of $[\text{Li}(\text{glyme})]^+$ complexes and their interactions with anions in equimolar mixtures of glymes and Li[TFSA]: analysis by molecular dynamics simulations. *Physical Chemistry Chemical Physics* **2014**, *17*, 126–129.

(20) Callsen, M.; Sodeyama, K.; Futera, Z.; Tateyama, Y.; Hamada, I. The solvation structure of lithium ions in an ether based electrolyte solution from first-principles molecular dynamics. *The Journal of Physical Chemistry B* **2017**, *121*, 180–188.

(21) Sun, Y.; Hamada, I. Insight into the solvation structure of tetraglyme-based electrolytes via first-principles molecular dynamics simulation. *The Journal of Physical Chemistry B* **2018**, *122*, 10014–10022.

(22) Zhang, C.; Ueno, K.; Yamazaki, A.; Yoshida, K.; Moon, H.; Mandai, T.; Umebayashi, Y.; Dokko, K.; Watanabe, M. Chelate Effects in Glyme/Lithium Bis(trifluoromethanesulfonyl)amide Solvate Ionic Liquids. I. Stability of Solvate Cations

and Correlation with Electrolyte Properties. *The Journal of Physical Chemistry B* **2014**, *118*, 5144–5153.

(23) Ho, J. S.; Borodin, O. A.; Ding, M. S.; Ma, L.; Schroeder, M. A.; Pastel, G. R.; Xu, K. Understanding Lithium-ion Transport in Sulfolane-and Tetraglyme-Based Electrolytes Using Very Low-Frequency Impedance Spectroscopy. *Energy & Environmental Materials* **2023**, *6*, e12302.

(24) Rajput, N. N.; Qu, X.; Sa, N.; Burrell, A. K.; Persson, K. A. The coupling between stability and ion pair formation in magnesium electrolytes from first-principles quantum mechanics and classical molecular dynamics. *Journal of the American Chemical Society* **2015**, *137*, 3411–3420.

(25) Rushing, J. C.; Leonik, F. M.; Kuroda, D. G. Effect of solvation shell structure and composition on ion pair formation: The case study of litdi in organic carbonates. *The Journal of Physical Chemistry C* **2019**, *123*, 25102–25112.

(26) Galvez-Aranda, D. E.; Seminario, J. M. Ion pairing, clustering and transport in a LiFSI-TMP electrolyte as functions of salt concentration using molecular dynamics simulations. *Journal of The Electrochemical Society* **2021**, *168*, 040511.

(27) Chen, X.; Li, Z.; Zhao, H.; Li, J.; Li, W.; Han, C.; Zhang, Y.; Lu, L.; Li, J.; Qiu, X. Dominant solvent-separated ion pairs in electrolytes enable superhigh conductivity for fast-charging and low-temperature lithium ion batteries. *ACS nano* **2024**, *18*, 8350–8359.

(28) Tan, X.; Chen, M.; Zhang, J.; Li, S.; Zhang, H.; Yang, L.; Sun, T.; Qian, X.; Feng, G. Decoding Electrochemical Processes of Lithium-Ion Batteries by Classical Molecular Dynamics Simulations. *Advanced Energy Materials* **2024**, *14*, 2400564.

(29) Magdău, I.-B.; Arismendi-Arrieta, D. J.; Smith, H. E.; Grey, C. P.; Hermansson, K.; Csányi, G. Machine learning force fields for molecular liquids: Ethylene Carbon-

ate/Ethyl Methyl Carbonate binary solvent. *npj Computational Materials* **2023**, *9*, 146.

(30) Goodwin, Z. A.; Wenny, M. B.; Yang, J. H.; Cepellotti, A.; Ding, J.; Bystrom, K.; Duschatko, B. R.; Johansson, A.; Sun, L.; Batzner, S.; others Transferability and accuracy of ionic liquid simulations with equivariant machine learning interatomic potentials. *The Journal of Physical Chemistry Letters* **2024**, *15*, 7539–7547.

(31) Gong, S.; Zhang, Y.; Mu, Z.; Pu, Z.; Wang, H.; Han, X.; Yu, Z.; Chen, M.; Zheng, T.; Wang, Z.; others A predictive machine learning force-field framework for liquid electrolyte development. *Nature Machine Intelligence* **2025**, 1–10.

(32) Levine, D. S.; Shuaibi, M.; Spotte-Smith, E. W. C.; Taylor, M. G.; Hasyim, M. R.; Michel, K.; Batatia, I.; Csányi, G.; Dzamba, M.; Eastman, P.; others The open molecules 2025 (omol25) dataset, evaluations, and models. *arXiv preprint arXiv:2505.08762* **2025**,

(33) Harte, T.; Dharmasiri, B.; Dobhal, G. S.; Walsh, T. R.; Henderson, L. C. Accelerated lithium-ion diffusion via a ligand ‘hopping’ mechanism in lithium enriched solvate ionic liquids. *Physical Chemistry Chemical Physics* **2023**, *25*, 29614–29623.

(34) Thum, A.; Heuer, A.; Shimizu, K.; Lopes, J. N. C. Solvate ionic liquids based on lithium bis(trifluoromethanesulfonyl)imide-glyme systems: Coordination in MD simulations with scaled charges. *Physical Chemistry Chemical Physics* **2020**, *22*, 525–535.

(35) Mitra, S.; Biswas, R. Exploring the capabilities and limitations of the Van Hove function to understand directional correlations in ion movements within Li-ion battery electrolytes. *The Journal of Chemical Physics* **2024**, *161*.

(36) Philippi, F.; Matsuyama, Y.; Buyting, S.; Sudoh, T.; Shigenobu, K.; Shinoda, W.; Schönhoff, M.; Watanabe, M.; Ueno, K. Discrepant lithium transference numbers due to heterogeneous speciation. *Phys. Chem. Chem. Phys.* **2025**, *27*, 15185–15195.

(37) Nayak, R. G.; Mallik, B. S. Heterogeneous microstructures and dynamics of the Li-ion electrolyte with a fluorinated additive solvent from molecular dynamics simulations. *Phys. Chem. Chem. Phys.* **2025**, *27*, 14264–14276.

(38) Jorgensen, W. L.; Maxwell, D. S.; Tirado-Rives, J. Development and testing of the OPLS all-atom force field on conformational energetics and properties of organic liquids. *Journal of the american chemical society* **1996**, *118*, 11225–11236.

(39) Chai, J.-D.; Head-Gordon, M. Systematic optimization of long-range corrected hybrid density functionals. *The Journal of Chemical Physics* **2008**, *128*, 084106.

(40) Caldeweyher, E.; Bannwarth, C.; Grimme, S. Extension of the D3 dispersion coefficient model. *The Journal of Chemical Physics* **2017**, *147*, 034112.

(41) Neese, F. Software update: the ORCA program system, version 5.0. *WIRES Comput. Molec. Sci.* **2022**, *12*, e1606.

(42) Breneman, C. M.; Wiberg, K. B. Determining atom-centered monopoles from molecular electrostatic potentials. The need for high sampling density in formamide conformational analysis. *Journal of Computational Chemistry* **1990**, *11*, 361–373.

(43) Essmann, U.; Perera, L.; Berkowitz, M. L.; Darden, T.; Lee, H.; Pedersen, L. G. A smooth particle mesh Ewald method. *The Journal of chemical physics* **1995**, *103*, 8577–8593.

(44) Abraham, M. J.; Murtola, T.; Schulz, R.; Páll, S.; Smith, J. C.; Hess, B.; Lindahl, E. GROMACS: High performance molecular simulations through multi-level parallelism from laptops to supercomputers. *SoftwareX* **2015**, *1-2*, 19–25.

(45) Humphrey, W.; Dalke, A.; Schulten, K. VMD: visual molecular dynamics. *Journal of molecular graphics* **1996**, *14*, 33–38.

(46) Brehm, M.; Thomas, M.; Gehrke, S.; Kirchner, B. TRAVIS—A free analyzer for trajectories from molecular simulation. *The Journal of Chemical Physics* **2020**, *152*, 164105.

(47) Bussi, G.; Donadio, D.; Parrinello, M. Canonical sampling through velocity rescaling. *The Journal of Chemical Physics* **2007**, *126*, 014101.

(48) Berendsen, H. J.; Postma, J. v.; Van Gunsteren, W. F.; DiNola, A.; Haak, J. R. Molecular dynamics with coupling to an external bath. *The Journal of chemical physics* **1984**, *81*, 3684–3690.

(49) Murphy, T.; Callear, S. K.; Yepuri, N.; Shimizu, K.; Watanabe, M.; Lopes, J. N. C.; Darwish, T.; Warr, G. G.; Atkin, R. Bulk nanostructure of the prototypical ‘good’ and ‘poor’ solvate ionic liquids $[\text{Li}(\text{G4})][\text{TFSI}]$ and $[\text{Li}(\text{G4})][\text{NO}_3]$. *Physical Chemistry Chemical Physics* **2016**, *18*, 17224–17236.

(50) Ueno, K.; Yoshida, K.; Tsuchiya, M.; Tachikawa, N.; Dokko, K.; Watanabe, M. Glyme–lithium salt equimolar molten mixtures: concentrated solutions or solvate ionic liquids? *The Journal of Physical Chemistry B* **2012**, *116*, 11323–11331.

(51) Shinoda, W.; Hatanaka, Y.; Hirakawa, M.; Okazaki, S.; Tsuzuki, S.; Ueno, K.; Watanabe, M. Molecular dynamics study of thermodynamic stability and dynamics of $[\text{Li}(\text{glyme})]^+$ complex in lithium-glyme solvate ionic liquids. *The Journal of Chemical Physics* **2018**, *148*.

(52) Fall, B.; Sonnenberg, L. A.; Aguirre, J. R.; Paul, S. C.; Prakash, P.; Venkatnathan, A.; Garaga, M. N.; Goddard III, W. A.; Greenbaum, S. G.; Zdilla, M. J.; Wunder, S. L. Effect of Anion Mass on Conductivity and Lithium-Ion Transference Number in the Isomorphic Cocrystals $(\text{Adpn})_2\text{LiXF}_6$ ($\text{Adpn} = \text{Adiponitrile}$, $\text{X} = \text{P, As, Sb}$). *Chemistry of Materials* **2025**, *37*, 1798–1809.

(53) Paul, S. C.; Goddard, W. A.; Zdilla, M.; Prakash, P.; Wunder, S. L. Grain boundary

tuning determines iodide and lithium-ion migration in a solid adiponitrile–LiI molecular crystal electrolyte. *Mater. Horiz.* **2025**, *12*, 10728–10739.

(54) Shigenobu, K.; Dokko, K.; Watanabe, M.; Ueno, K. Solvent effects on Li ion transference number and dynamic ion correlations in glyme- and sulfolane-based molten Li salt solvates. *Phys. Chem. Chem. Phys.* **2020**, *22*, 15214–15221.

(55) Sudoh, T.; Shigenobu, K.; Dokko, K.; Watanabe, M.; Ueno, K. Li⁺ transference number and dynamic ion correlations in glyme-Li salt solvate ionic liquids diluted with molecular solvents. *Phys. Chem. Chem. Phys.* **2022**, *24*, 14269–14276.

(56) Saito, M.; Yamada, S.; Ishikawa, T.; Otsuka, H.; Ito, K.; Kubo, Y. Factors influencing fast ion transport in glyme-based electrolytes for rechargeable lithium–air batteries. *RSC Adv.* **2017**, *7*, 49031–49040.

(57) Zhang, Y.; Maginn, E. J. Water-In-Salt LiTFSI Aqueous Electrolytes (2): Transport Properties and Li⁺ Dynamics Based on Molecular Dynamics Simulations. *The Journal of Physical Chemistry B* **2021**, *125*, 13246–13254.

(58) Krucker-Velasquez, E.; Swan, J. W. Underscreening and hidden ion structures in large scale simulations of concentrated electrolytes. *The Journal of Chemical Physics* **2021**, *155*, 134903.

(59) Dinpajoooh, M.; Intan, N. N.; Duignan, T. T.; Biasin, E.; Fulton, J. L.; Kathmann, S. M.; Schenter, G. K.; Mundy, C. J. Beyond the Debye–Hückel limit: Toward a general theory for concentrated electrolytes. *The Journal of Chemical Physics* **2024**, *161*, 230901.